definitions of ξ and τ from Eq. (23), Eq. (38) indicates that ω_t, and hence the coning angle, grows or decays depending on the sign of T.

References

[1] Iorillo, A. J., "Nutation Damping Dynamics of Axisymmetric Rotor Stabilized Satellites," ASME Winter Meeting, Chicago, Ill., Nov. 1959.

[2] Likins, P. W., "Attitude Stability Criteria for Dual Spin Spacecraft," *Journal of Spacecraft and Rockets*, Vol. 4, No. 12, Dec. 1967, pp. 1638–1643.

[3] Mingori, D. L., "Effects of Energy Dissipation on the Attitude Stability of Dual-Spin Satellites," *AIAA Journal*, Vol. 7, No. 1, Jan. 1969, pp. 20–27.

[4] Pringle, R., Jr., "Stability of the Force-Free Motions of a Dual-Spin Spacecraft," *AIAA Journal*, Vol. 7, No. 6, June 1969, pp. 1054–1063.

[5] Velman, J. R., "Simulation Results for a Dual-Spin Spacecraft," *Proceedings of the Symposium on Attitude Stabilization and Control of Dual-Spin Spacecraft, Aug. 1–2, 1967*, Rept. SAMSO-TR-68-191, Nov. 1967, U. S. Air Force.

[6] Johnson, C. R., "Tacasat I Nutation Dynamics," to be published in *AIAA Progress in Astronautics and Aeronautics: Communications Satellite Technology for the 70's*, Vol. 25, edited by N. E. Feldman and C. M. Kelly, MIT Press, Cambridge, 1971.

MAY 1971 AIAA JOURNAL VOL. 9, NO. 5

Large Deformation, Deep Penetration Theory for a Compressible Strain-Hardening Target Material

SATHYA HANAGUD*
Georgia Institute of Technology, Atlanta, Ga.

AND

BERNARD ROSS†
Failure Analysis Associates, Stanford, Calif.

Hypervelocity impact of a rigid spherical projectile with a compressible target material is investigated. Analytic solutions obtained for this problem are based on dynamic cavity expansion and Goodier deep penetration theories and are not restricted, as in previous work, to an incompressible medium. Target compressibility is introduced through a locking approximation for real material behavior under hydrostatic stress. In particular, values of locking density are obtained from Hugoniot curves characterizing homogeneous, isotropic material behavior at different impact velocities. Results of the theory indicate that terminal penetration depth is a function of projectile diameter and mass, and initial density, locking density, yield stress, and strain-hardening modulus of the target material. Using results of the theory, curves are plotted to show the comparison between compressible and incompressible penetration theory for the hypervelocity impact of steel projectiles on an aluminum target.

Nomenclature

A,D,M = cross section area, diameter, and mass of projectile, respectively
a = radius of spherical cavity
B_1,B_2 = constants related to dynamic pressure, see Eq. (71)
b = radius of locked-elastic, locked-plastic spherical shock front
C_1 = constant of integration
E,G = modulus of elasticity and shear modulus, respectively
E_t = tangent modulus for linear strain-hardening
e = bulk strain
$\bar{f}$ = limit of integration
f,g = functions of integration
k = radius of stress-free, locked-elastic spherical shock front
n = summation exponent
p_s = static pressure term given by Eq. (71)
$p(t)$ = dynamic pressure applied to spherical cavity surface as a function of time
$q,\dot{q},\ddot{q}$ = depth, velocity, and acceleration, respectively, of projectile in target material
q_0,v_0 = penetration depth and velocity of projectile after completion of shallow penetration phase
q_t = final penetration depth of projectile
r = Eulerian radial coordinate
t = time
v = outward particle velocity in radial direction
Y = yield stress
α = material constant given by Eqs. (16), (24)
β = material constant given by Eq. (40)
δ = material constant given by Eq. (66)
ϵ_1,ϵ_2 = small quantities in the mathematical sense
$\bar{\epsilon}_l$ = locking strain, $\bar{\epsilon}_l = -\epsilon_l$
$\epsilon_r,\epsilon_\theta$ = normal strains in radial and circumferential directions, respectively
η = series expression given by Eq. (54)
θ,φ = equatorial and meridional spherical coordinates, respectively
ρ,ρ_l = density and locking density of target material, respectively
σ_r,σ_θ = normal stresses inr adial and circumferential directions, respectively

Received January 26, 1970; revision received November 19, 1970. Work supported by the Naval Ordnance Laboratory, White Oak, Md. and the Office of Naval Research.

* Professor of Aerospace Engineering, (visiting), formerly Research Mathematician, Stanford Research Institute, Menlo Park, Calif., and at present a Senior Consultant to the Failure Analysis Associates.

† Engineer, Structural Mechanics, formerly Engineering Physicist, Stanford Research Institute, Menlo Park, Calif. Member AIAA.

Subscripts

e = locked-elastic region
p = locked-plastic region
0 = initial values and/or stress-free region

Introduction

THIS study treats the deep penetration behavior of a rigid spherical projectile following hypervelocity impact at normal incidence with a homogeneous, isotropic material. Solution of the problem is based on a combination of dynamic cavity expansion and deep penetration theories and in this connection is similar in concept and development to the work of Goodier.[1] However, Goodier's study was founded on the assumption that the target material is incompressible elastically as well as plastically, whereas in the present investigation the restriction to incompressibility is relaxed by a suitable approximation. Thus, a whole new class of target materials can be analyzed in substantially greater detail and the understanding of their dynamic response to hypervelocity impact increased. The Goodier approach is relatively simple in formulation and extremely useful because it furnishes analytic solutions in lieu of expensive numerical solutions that require lengthy computer codes.

Original synthesis of an explanation for the deep penetration problem based on cavity expansion theory was accomplished over 25 years ago by Bishop, Hill, and Mott[2] for the quasistatic punch indentation process (i.e., hardness testing theory under very slow loading rates). In this work, solutions concerning the static expansion of cylindrical and spherical cavities in an infinite medium were obtained. Extension to penetration problems under hypervelocity impact was carried out by Goodier[1] using results from the dynamic spherical cavity expansion studies reported in Hopkins.[3] In this case, Goodier also supplied the correct solution for a strain-hardening target material. Moreover, he showed that the influence of strain-hardening on penetration behavior at high rates of loading was extremely important and thus could not be neglected in hypervelocity impact problems. However, it was believed that neglect of compressibility in the existing solutions could also engender significant consequences in the theoretical dynamic response of many types of target materials under rapid loading conditions. Thus, the present work has attempted to introduce target compressibility to the problem through an idealized locking approximation for real material behavior under hydrostatic stress.[4] In this connection, appropriate values of locking density were related to impact velocity of the projectile through consideration of Hugoniot curves for the target medium. Then, the dynamic spherical cavity expansion problem was solved and results of this effort employed to obtain terminal penetration depths.

Briefly, in application of this method of approach the stresses in an infinite, homogeneous, isotropic solid containing a spherical cavity under suddenly applied and maintained uniform pressure are obtained using large-deformation theory where locking behavior in dilatation and elastic-plastic-strain-hardening behavior in shear are assumed. By making approximations similar to those of Goodier,[1,5] a solution is derived which yields a definitive relationship between pressure at the cavity surface and cavity radius. Subsequently, an assumed spatial variation of pressure at the projectile-target interface is used to calculate the total resisting force acting on the projectile. This in turn enables the equation of motion for the projectile in the resisting medium to be written so that suitable integration up to zero terminal velocity yields ultimately the maximum depth of penetration achieved.

Large Deformation, Deep Penetration Theory for a Locking Medium

The problem treated concerns a material that experiences two-phase, ideal-locking compressibility behavior under hydrostatic stress and elastic-plastic response with linear strain hardening under shear stress. As a result of these conditions, the sudden application of pressure at the cavity surface in the initially stress-free solid produces a surrounding spherical region of material that is instantaneously elastic locked in dilatation, and elastic in shear. Values of locking strain or locking density are obtained from the experimental Rankine-Hugoniot relationships which characterize material behavior under hydrostatic compression at high rates of loading. The elastic situation persists under increasing pressure until the yield stress is attained at the cavity surface whereupon the medium experiences plastic locking stresses in dilatation and plastic behavior in shear. At this point, values of hydrostatic stress for the locked-plastic material are greater than those values characteristic of the locked-elastic condition. Further increase of pressure with time causes the locked-plastic region surrounding the cavity to grow in extent so that the spherical surface which acts as a boundary between the initially generated locked-elastic material and the following zone of locked-plastic material propagates outward radially from the expanding cavity surface. The problem described is depicted schematically in Figs. 1 and 2. These sketches indicate characteristic idealized stress-strain material behavior curves, and show spatial relationships between the cavity, locked-plastic, and locked-elastic regions. Here, it is assumed that plastic locking occurs at the same instant as yielding.

In the following analysis, attention is directed first to the locked-elastic material in Region 1 (Fig. 2), which is behind the advancing shock wave at $r = k(t)$ where r is the Eulerian radial coordinate. Introducing the locking condition on strain

$$\epsilon_r + 2\epsilon_\theta = \epsilon_l \tag{1}$$

and noting that the associated strain rate quantities can be expressed in terms of the radial outward particle velocity $v(r,t)$ by the kinematic relations,

$$\dot{\epsilon}_r = \partial v/\partial r \quad \dot{\epsilon}_\theta = v/r \tag{2}$$

yields upon substitution and subsequent integration

$$v = f(t)/r^2 \tag{3}$$

where $f(t)$ is an unknown function. Next, the stress-strain relationship for an elastic material in shear is

$$\sigma_\theta - \sigma_r = 2G(\epsilon_\theta - \epsilon_r) \tag{4}$$

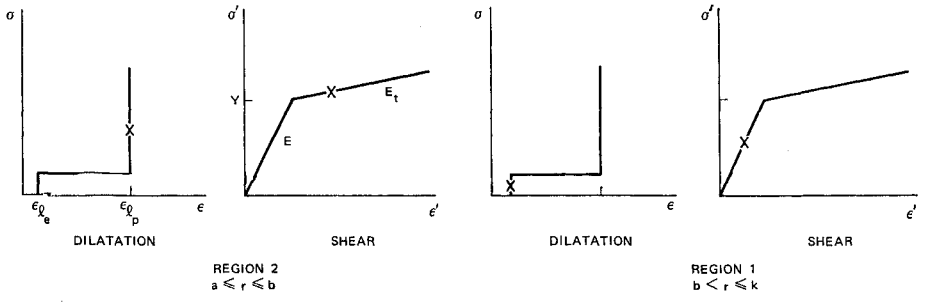

Fig. 1 Idealized stress-strain curves for a locking elastic-plastic material (X denotes applicable portion of stress-strain curve).

Moreover, if it is assumed that material in the locked-elastic state is ideally locked so that no further compressibility takes place; then, $G = E/3$ and Eq. (4) becomes

$$\sigma_\theta - \sigma_r = E(2\epsilon_\theta + 2\bar{\epsilon}_l/3) \tag{5}$$

where the circumferential strain quantity can be expressed for large deformations by

$$\epsilon_\theta = \ln r/r_0 \tag{6}$$

Now, the equation of motion under conditions of spherical symmetry is

$$(\partial\sigma_r/\partial r) + 2(\sigma_r - \sigma_\theta)/r = \rho Dv/Dt \tag{7}$$

where Dv/Dt refers to the total or Eulerian derivative of the particle velocity with respect to time along the particle path and is equal to

$$Dv/Dt = (\partial v/\partial t) + v\partial v/\partial r \tag{8}$$

Thus, Eqs. (3, 5, and 7) can be combined to yield

$$\frac{\partial\sigma_r}{\partial r} = \frac{2}{r}E\left(2\ln\frac{r}{r_0} + \frac{2\bar{\epsilon}_l}{3}\right) + \rho_l\left(\frac{\dot{f}}{r^2} - 2\frac{f^2}{r^5}\right) \tag{9}$$

whence integration results in

$$\sigma_{r_e} = 2\int_{\bar{f}_e}^{r}\frac{1}{r'}E\left(2\ln\frac{r'}{r_0} + \frac{2\bar{\epsilon}_{l_e}}{3}\right)dr' - \rho_{l_e}\frac{\dot{f}_e}{r} + \frac{1}{2}\rho_{l_e}\frac{f_e^2}{r^4} + g_e(t) \tag{10}$$

where the subscript e has been added to denote that quantities refer to the locked-elastic region.

Now, turning to the locked-plastic material shown as Region 2 in Fig. 2, it is noted that the ideal locking condition expressed by Eq. (1) remains applicable; however, the stress-strain relationship after yield for an elastic-plastic material with linear strain hardening is assumed in the following form:

$$\sigma_\theta - \sigma_r = Y + \tfrac{2}{3}E_t(\epsilon_\theta - \epsilon_r) \tag{11}$$

Using Eqs. (3, 6, 7, and 11), the following expression is obtained:

$$\frac{\partial\sigma_r}{\partial r} = \frac{2}{r}Y + \frac{2}{r}E_t(2\ln r/r_0 + 2\bar{\epsilon}_l/3) + \rho_l\frac{\dot{f}}{r^2} - 2\rho_l\frac{f^2}{r^5} \tag{12}$$

and after integration, there results

$$\sigma_{r_p} = 2Y\ln r + 2\int_{\bar{f}_p}^{r}\frac{1}{r'}E_t\left(2\ln\frac{r'}{r_0} + \frac{2\bar{\epsilon}_{l_p}}{3}\right)dr' - \rho_{l_p}\frac{\dot{f}_p}{r} + \frac{1}{2}\rho_{l_p}\frac{f_p^2}{r^4} + g_p(t) \tag{13}$$

where the subscript p has been added to indicate that quantities refer to the locked-plastic region.

Application of the conservation of mass principle at the leading shock front results in

$$\rho_0(\dot{k} - v_0) = \rho_{l_e}(\dot{k} - v_e) \qquad \text{at } r = k(t) \tag{14}$$

However, the particle velocity v_0 in the stress-free region ahead of the advancing shock is zero everywhere; therefore, Eqs. (3) and (14) yield

$$f_e(t) = \alpha_e k^2\dot{k} \tag{15}$$

where

$$\alpha_e = 1 - \rho_0/\rho_{l_e} \tag{16}$$

But, on the elastic-plastic interface at $r = b(t)$, the elastic stresses are in a state of incipient plasticity; thus, the yield condition must be satisfied at this location. That is,

$$\sigma_{\theta_e} - \sigma_{r_e} = Y \qquad \text{at } r = b(t) \tag{17}$$

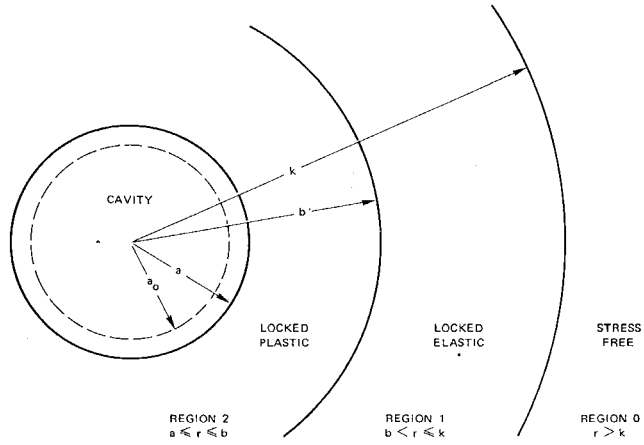

Fig. 2 Dynamic cavity expansion problem for a locking elastic-plastic material.

or substituting from Eq. (5),

$$\ln b/b_0 = (Y/2E) - \bar{\epsilon}_{l_e}/3 \qquad \text{at } r = b(t) \tag{18}$$

Within the locked-plastic zone, the following boundary condition can be applied at the cavity surface:

$$\sigma_{r_p} = -p(t) \qquad \text{at } r = a(t) \tag{19}$$

Then, from Eq. (13),

$$2Y\ln a + 2\int_{\bar{f}_p}^{a}\frac{1}{r'}E_t\left(2\ln\frac{r'}{r_0} + \frac{2\bar{\epsilon}_{l_p}}{3}\right)dr' - \rho_{l_p}\frac{\dot{f}_p}{a} + \frac{1}{2}\rho_{l_p}\frac{f_p^2}{a^4} + g_p(t) = -p(t) \quad \text{at} \quad r = a(t) \tag{20}$$

Next, solving Eq. (20) for the function, $g_p(t)$ and recombining with Eq. (13) results in

$$\sigma_{r_p} = -p(t) + 2Y\ln\frac{r}{a} + 2\int_{a}^{r}\frac{1}{r'}E_t\left(2\ln\frac{r'}{r_0} + \frac{2\bar{\epsilon}_{l_p}}{3}\right)dr' + \rho_{l_p}\dot{f}_p\left(\frac{1}{a} - \frac{1}{r}\right) - \frac{1}{2}\rho_{l_p}f_p^2\left(\frac{1}{a^4} - \frac{1}{r^4}\right) \tag{21}$$

The jump condition expressing the conservation of mass principle can be applied on the shock front at the elastic-plastic interface. There results,

$$\rho_{l_p}(\dot{b} - v_p) = \rho_{l_e}(\dot{b} - v_e) \qquad \text{at } r = b(t) \tag{22}$$

or using Eq. (3) in appropriate elastic and plastic regions

$$f_p(t) = \alpha_p b^2\dot{b} + (1 - \alpha_p)f_e(t) \tag{23}$$

where

$$\alpha_p = 1 - \rho_{l_e}/\rho_{l_p} \tag{24}$$

Now, the jump condition expressing the conservation of momentum principle is applied at the shock front as follows:

$$\sigma_{r_p} - \sigma_{r_e} = -\rho_{l_p}(\dot{b} - v_p)v_p + \rho_{l_e}(\dot{b} - v_e)v_e \qquad \text{at } r = b(t) \tag{25}$$

Substitution of Eqs. (3, 15, 22, 23) in Eq. (25) yields

$$\sigma_{r_p} - \sigma_{r_e}|_{r=b} = \rho_{l_e}\left(\dot{b} - \alpha_e\frac{k^2\dot{k}}{b^2}\right)\left(\alpha_e\frac{k^2\dot{k}}{b^2} - \alpha_p\dot{b} - (1 - \alpha_p)\alpha_e\frac{k^2\dot{k}}{b^2}\right) \tag{26}$$

which can be rewritten as

$$\sigma_{r_p} - \sigma_{r_e}|_{r=b} = \rho_{l_e}\left(-\alpha_p\dot{b}^2 + 2\alpha_e\alpha_p\frac{k^2\dot{k}\dot{b}}{b^2} - \alpha_e^2\alpha_p\frac{k^4\dot{k}^2}{b^4}\right) \quad (27)$$

Substitution of Eqs. (10), (21), in Eq. (27) gives

$$-p(t) + 2Y\ln\frac{b}{a} + 2\int_a^b\frac{1}{r'}E_t\left(2\ln\frac{r'}{r_0} + \frac{2\bar{\epsilon}_{l_p}}{3}\right)dr' + \rho_{l_p}\dot{f}_p\left(\frac{1}{a} - \frac{1}{b}\right) - \frac{1}{2}\rho_{l_p}f_p{}^2\left(\frac{1}{a^4} - \frac{1}{b^4}\right) + \rho_{l_e}\frac{\dot{f}_e}{b} - \frac{1}{2}\rho_{l_e}\frac{f_e^2}{b^4} - 2\int_{\bar{f}_e}^b\frac{1}{r'}E\left(2\ln\frac{r'}{r_0} + \frac{2\bar{\epsilon}_{l_e}}{3}\right)dr' - g_e(t) = \rho_{l_e}\left(-\alpha_p\dot{b}^2 + 2\alpha_e\alpha_p\frac{k^2\dot{k}\dot{b}}{b^2} - \alpha^2{}_e\alpha_p\frac{k^4\dot{k}^2}{b^4}\right) \quad \text{at } r = b(t) \quad (28)$$

whereupon solving Eq. (28) for the function, $g_e(t)$ and recombining with Eq. (10) results in

$$\sigma_{r_e} = -p(t) + 2Y\ln\frac{b}{a} + 2\int_b^a\frac{1}{r'}E_t\left(2\ln\frac{r'}{r_0} + \frac{2\bar{\epsilon}_{l_p}}{3}\right)dr' + \rho_{l_e}\left(\alpha_p\dot{b}^2 - 2\alpha_e\alpha_p\frac{k^2\dot{k}\dot{b}}{b^2} + \alpha_e^2\alpha_p\frac{k^4\dot{k}^2}{b^4}\right) + \rho_{l_p}\dot{f}_p\left(\frac{1}{a} - \frac{1}{b}\right) - \frac{1}{2}\rho_{l_p}f_p{}^2\left(\frac{1}{a^4} - \frac{1}{b^4}\right) + \rho_{l_e}\dot{f}_e\left(\frac{1}{b} - \frac{1}{r}\right) - \frac{1}{2}\rho_{l_e}f_e{}^2\left(\frac{1}{b^4} - \frac{1}{r^4}\right) + 2\int_b^r\frac{1}{r'}E\left(2\ln\frac{r'}{r_0} + \frac{2\bar{\epsilon}_{l_e}}{3}\right)dr' \quad (29)$$

where

$$\dot{f}_e = \alpha_e k^2\ddot{k} + 2\alpha_e k\dot{k}^2 \quad (30)$$

$$\dot{f}_p = \alpha_p b^2\ddot{b} + 2\alpha_p b\dot{b}^2 + (1 - \alpha_p)(\alpha_e k^2\ddot{k} + 2\alpha_e k\dot{k}^2) \quad (31)$$

The jump condition expressing the conservation of momentum principle can be applied across the leading shock front;

$$\sigma_{r_e} - \sigma_{r_0} = -\rho_{l_e}(\dot{k} - v_e)v_e + \rho_0(\dot{k} - v_0)v_0 \qquad \text{at } r = k(t) \quad (32)$$

However, in the stress-free region ahead of the shock front, the stress σ_{r_0} and particle velocity v_0 are zero everywhere. Thus, with the use of Eqs. (14) and (15),

$$\sigma_{r_e} = -\rho_{l_e}(\dot{k} - \alpha_e\dot{k})\alpha_e\dot{k} \qquad \text{at } r = k(t) \quad (33)$$

Then, substitution of Eqs. (24, 30, 31, 33) in Eq. (29) results in an expression for the time variation of pressure at the cavity surface. That is,

$$p(t) = 2Y\ln\frac{b}{a} + 2\int_a^b\frac{1}{r'}E_t\left(2\ln\frac{r'}{r_0} + \frac{2\bar{\epsilon}_{l_p}}{3}\right)dr' + \alpha_p\rho_{l_e}\left(\dot{b} - \alpha_e\frac{k^2\dot{k}}{b^2}\right)^2 + \alpha_e\rho_{l_e}(k^2\ddot{k} + 2k\dot{k}^2)\left(\frac{1}{a} - \frac{1}{k}\right) - \alpha_p\rho_{l_p}(b\ddot{b}^2 + 2b\dot{b}^2)\left(\frac{1}{a} - \frac{1}{b}\right) - \frac{1}{2}\rho_{l_p}f_p{}^2\left(\frac{1}{a^4} - \frac{1}{b^4}\right) - \frac{1}{2}\rho_{l_e}f_e{}^2\left(\frac{1}{b^4} - \frac{1}{k^4}\right) + 2\int_b^k\frac{1}{r'}E\left(2\ln\frac{r'}{r_0} + \frac{2\bar{\epsilon}_{l_e}}{3}\right)\times dr' + \rho_0\alpha_e\dot{k}^2 \quad (34)$$

It is assumed that the leading shock front at $r = k(t)$ is relatively weak, such that the elastic locking strain ϵ_{l_e} and concomitant jump in density from the stress-free region to the locked-elastic region are very small, (i.e., elastic strains are small compared to plastic strains). Then, the following relationships hold:

$$\bar{\epsilon}_{l_e} \approx 0 \quad \rho_0 \approx \rho_{l_e} \quad (35)$$

$$\therefore f_e \approx 0 \quad \alpha_e = 1 - (\rho_0/\rho_{l_e}) \quad (36)$$

and

$$\alpha_p = 1 - \frac{\rho_{l_e}}{\rho_{l_p}} \approx 1 - \frac{\rho_0}{\rho_{l_p}} \quad (37)$$

Then, the expression for $p(t)$ given by Eq. (34) becomes

$$p(t) = 2Y\ln\frac{b}{a} + 2\int_a^b\frac{1}{r'}E_t\left(2\ln\frac{r'}{r_0} + \frac{2\bar{\epsilon}_{l_p}}{3}\right)dr' + \alpha_p\rho_0\dot{b}^2 + \alpha_p\rho_{l_p}(b^2\ddot{b} + 2b\dot{b}^2)\left(\frac{1}{a} - \frac{1}{b}\right) - \frac{1}{2}\rho_{l_p}f_p{}^2\left(\frac{1}{a^4} - \frac{1}{b^4}\right) + 2\int_b^k\frac{1}{r'}E\left(2\ln\frac{r'}{r_0}\right)dr' \quad (38)$$

However, Eqs. (15) and (23) can be employed to obtain

$$f_p{}^2 = \alpha_p{}^2b^4\dot{b}^2 \quad (39)$$

Introducing the yield condition given by Eq. (18) and a new parameter β, such that‡

$$\ln b/b_0 = (Y/2E) - \bar{\epsilon}_{l_e}/3 = \beta \quad (40)$$

it follows that

$$b_0 = b/e^\beta \quad (41)$$

Next, consideration of compressibility in the locked-elastic region, $b(t) < r \leq k(t)$, over an arbitrary time period $t' = t_0$ $(b' = b_0, r' = r_0)$, $t' = t$ $(b' = b, r' = r)$, and subsequent application of the conservation of mass principle yields

$$(r^3 - b^3)\rho_{l_e} = (r_0{}^3 - b_0{}^3)\rho_0 \quad (42)$$

or with the use of Eq. (41),

$$\frac{r_0}{r} = \left[1 - \frac{b^3}{r^3}\left(1 - e^{-3\beta}\frac{\rho_0}{\rho_{l_e}}\right)\right]^{1/3}\left[\frac{\rho_{l_e}}{\rho_0}\right]^{1/3} \quad (43)$$

Now, the exponential function $e^{-3\beta}$ can be expanded in series form so that under the weak shock condition (i.e., $\rho_0 \approx \rho_{l_e}$), Eq. (43) becomes

$$r_0/r = [1 - (b^3/r^3)(3\beta - \tfrac{9}{2}\beta^2 + \ldots)]^{1/3} \quad (44)$$

Then, referring back to Eq. (38), the following relationship applies to the logarithmic term:

$$\ln\frac{r'}{r_0} = -\ln\left[1 - \frac{b^3}{r^3}\left(3\beta - \frac{9}{2}\beta^2 + \ldots\right)\right]^{1/3} \approx \frac{1}{3}\left\{\frac{b^3}{r'^3}\left(3\beta - \frac{9}{2}\beta^2 + \ldots\right)\right\} \quad (45)$$

where it has been assumed that $E \gg Y$, so that $\beta \ll 1$ and for the region $b < r' \leq k$ the quantity

$$b^3/r'^3(3\beta - \tfrac{9}{2}\beta^2 + \ldots) \ll 1 \quad (46)$$

Turning to the integral expression in Eq. (38) and using Eq. (45) results in

$$2\int_b^k\frac{1}{r'}E\left(2\ln\frac{r'}{r_0}\right)dr' = \frac{4}{3}E\int_b^k\frac{b^3}{r'^4}\times\left(3\beta - \frac{9}{2}\beta^2 + \ldots\right)dr' = \frac{4}{9}Eb^3\times\left(3\beta - \frac{9}{2}\beta^2 + \ldots\right)\left(\frac{1}{b^3} - \frac{1}{k^3}\right) \quad (47)$$

‡ The quantities $\bar{\epsilon}_{l_e}$ and ρ_{l_e} are retained for the present. Approximations, $\bar{\epsilon}_{l_e} \approx 0$ and $\rho_{l_e} \approx \rho_0$, will be reintroduced at a later stage.

However, for $\bar{\epsilon}_{l_e} \approx 0$, the radial distance, $k \to \infty$. Thus, Eq. (47) reduces to

$$2\int_b^k \frac{1}{r'} E\left(2\ln\frac{r'}{r_0}\right) dr' = \frac{4}{9}E\left(3\beta - \frac{9}{2}\beta^2 + \ldots\right) = E(1 - e^{-3\beta}) \quad (48)$$

Consideration of compressibility in the locked-plastic region, $a(t) < r \leq b(t)$, under conditions similar to those employed in obtaining Eq. (42) provides

$$(b^3 - a^3)\rho_{l_p} = (b_0^3 - a_0^3)\rho_{l_e} \quad (49)$$

or using Eq. (41) again,

$$\frac{b^3}{a^3}\left(1 - e^{-2\beta}\frac{\rho_{l_e}}{\rho_{l_p}}\right) = 1 - \frac{a_0^3}{a^3}\frac{\rho_{l_e}}{\rho_{l_p}} \quad (50)$$

But it has been shown by Goodier[1] that for the deep penetration problem (i.e., penetration depths greater than 4–5 projectile diam), $a^3 \gg a_0^3$. In addition, under present conditions, $\rho_{l_e} \approx \rho_0$ and $\rho_{l_e} < \rho_{l_p}$. Thus, Eq. (50) can be written as

$$b/a = (1 - e^{-3\beta}\rho_0/\rho_{l_p})^{-1/3} \quad (51)$$

and it follows that

$$2Y \ln b/a = -\tfrac{2}{3}Y \ln(1 - e^{-3\beta}\rho_0/\rho_{l_p}) \quad (52)$$

Finally, it is noted that the remaining integral in Eq. (38) has been evaluated in Ref. 6, and is given by

$$2\int_a^b \frac{1}{r'} E_t\left(2\ln\frac{r'}{r_0} + \frac{2\bar{\epsilon}_{l_p}}{3}\right) dr' = \frac{2}{27}\pi^2 E_t - \frac{4}{9}E_t\eta \quad (53)$$

where

$$\eta = \sum_{n=1}^{\infty}\frac{1}{n^2}\left(1 - e^{-3\beta}\frac{\rho_0}{\rho_{l_p}}\right)^n \quad (54)$$

Now, if Eqs. (39, 48, 52, and 53) are substituted in Eq. (38), there results,

$$p(t) = -\frac{2}{3}Y\ln\left(1 - e^{-3\beta}\frac{\rho_0}{\rho_{l_p}}\right) + \frac{2}{27}\pi^2 E_t - \frac{4}{9}E_t\eta + \alpha_p\rho_0\dot{b}^2 + \alpha_p\rho_{l_p}(b\ddot{b} + 2\dot{b}^2)\left(\frac{b}{a} - 1\right) - \frac{1}{2}\alpha_p^2\rho_{l_p}\dot{b}^2\left(\frac{b^4}{a^4} - 1\right) + \frac{4}{9}E(1 - e^{-3\beta}) \quad (55)$$

A relationship between b and a can be obtained by employing the condition that the particle velocity at the spherical cavity surface must be equal to the time rate of change of cavity radius. That is

$$v_p(t) = \dot{a} \qquad \text{at } r = a(t) \quad (56)$$

Moreover, application of Eq. (3) to the plastic region gives

$$f_p(t) = a^2\dot{a} \quad (57)$$

or combining Eqs. (39) and (57)

$$\alpha_p\dot{b} = a^2\dot{a}/b^2 \quad (58)$$

Furthermore, with the use of Eq. (51), the following result is derived:

$$\alpha_p\rho_0\dot{b}^2 = \frac{a^2}{b^2}\dot{a}\rho_0\dot{b} = \left(1 - e^{-3\beta}\frac{\rho_0}{\rho_{l_p}}\right)^{2/3} \times \dot{a}^2\left(1 - e^{-3\beta}\frac{\rho_0}{\rho_{l_p}}\right)^{-1/3}\rho_0 = \rho_0\dot{a}^2\left(1 - e^{-3\beta}\frac{\rho_0}{\rho_{l_p}}\right)^{1/3} \quad (59)$$

But, it can be demonstrated by alternate manipulation of Eq. (51) and the expression given in Eq. (59) that

$$\alpha_p = (1 - e^{-3\beta}\rho_0/\rho_{l_p}) \quad (60)$$

This result is seemingly inconsistent with the definition of α_p contained in Eq. (24); however, it follows as a consequence of the assumption that $a^3 \gg a_0^3$. In reality, the term β is usually $\ll 1$ so that $e^{-3\beta} \approx 1$ and the original definition of α_p is preserved. Under these circumstances, it appears anomalous to effect distinction between the separate expressions for α_p given by Eqs. (24) and (60). On the other hand, in problems where material compressibility is either neglected (i.e., $\rho_0/\rho_{l_p} = 1$) or is small but finite (i.e., $\rho_0/\rho_{l_p} \approx 1$), the quantities under consideration can be represented by

$$1 - e^{-3\beta}\rho_0/\rho_{l_p} \approx \epsilon_1 \quad 1 - (\rho_0/\rho_{l_p}) \approx \epsilon_2$$

where ϵ_1 and ϵ_2 are both small in the mathematical sense. Now, it will be shown later that the term $\ln \epsilon_1$ appears in the final expression for dynamic cavity pressure. In this case, even though the magnitudes of ϵ_1 and ϵ_2 are approximately equal, the magnitudes of their respective natural logarithms are not; therefore, individual identities of these terms must be retained. Returning to Eq. (58),

$$\dot{(a^2\dot{a})} = \dot{(\alpha_p\dot{b}^2 b)} \quad (61)$$

or

$$a^2\ddot{a} + 2a\dot{a}^2 = \alpha_p(b^2\ddot{b} + 2b\dot{b}^2) \quad (62)$$

Substitution of these results into Eq. (55) yields

$$p(t) = \frac{4}{9}E(1 - e^{-3\beta}) - \frac{2}{3}Y\ln\left(1 - e^{-3\beta}\frac{\rho_0}{\rho_{l_p}}\right) + \frac{2}{27}\pi^2 E_t - \frac{4}{9}E_t\eta + \rho_{l_p}(a\ddot{a} + 2\dot{a}^2)\left(1 - \frac{a}{b}\right) - \frac{1}{2}\rho_{l_p}\dot{a}^2\left(1 - \frac{a^4}{b^4}\right) + \rho_0\dot{a}^2\left(1 - e^{-3\beta}\frac{\rho_0}{\rho_{l_p}}\right)^{1/3} \quad (63)$$

It is apparent that the static and dynamic pressure terms in Eq. (63) can be separated, and for this purpose it is convenient to represent static terms by the quantity p_s where

$$p_s = \frac{4}{9}E(1 - e^{-3\beta}) - \frac{2}{3}Y\ln\left(1 - e^{-3\beta}\frac{\rho_0}{\rho_{l_p}}\right) + \frac{2}{27}\pi^2 E_t - \frac{4}{9}E_t\eta \quad (64)$$

Thus, Eq. (63) becomes with the use of Eqs. (51), (64),

$$p(t) = p_s + \rho_{l_p}\left\{a\ddot{a}(1 - \delta^{1/3}) + \dot{a}^2\left[2(1 - \delta^{1/3}) - \frac{1}{2}(1 - \delta^{4/3}) + \frac{\rho_0}{\rho_{l_p}}\delta^{1/3}\right]\right\} \quad (65)$$

where

$$\delta = (1 - e^{-3\beta}\rho_0/\rho_{l_p}) \quad (66)$$

At this point, it is useful to compare the expression for pressure $p(t)$ at the cavity surface given by Eq. (65) with the relationship obtained by Goodier[1,5] for the corresponding spherical cavity expansion problem in an incompressible medium. In the latter case,

$$\bar{\epsilon}_{l_e} = \bar{\epsilon}_{l_p} = 0 \quad \text{and} \quad \rho_{l_p} = \rho_0 = \rho \quad (67)$$

With the introduction of these conditions, Eq. (64) can be written in the following way:

$$p_s \simeq \frac{4}{9}E(3\beta) + \frac{2}{3}Y\ln\left(\frac{1}{3\beta}\right) + \frac{2}{27}\pi^2 E_t - \frac{4}{9}E_t(3\beta) \quad (68)$$

or utilizing Eq. (40) for $\bar{\epsilon}_{l_e} = 0$,

$$p_s = \tfrac{2}{3}Y(1 + \ln 2E/3Y) + \tfrac{2}{27}\pi^2 E_t - \tfrac{2}{3}(E_t Y/E) \quad (69)$$

Employing similar manipulation for the dynamic portion of

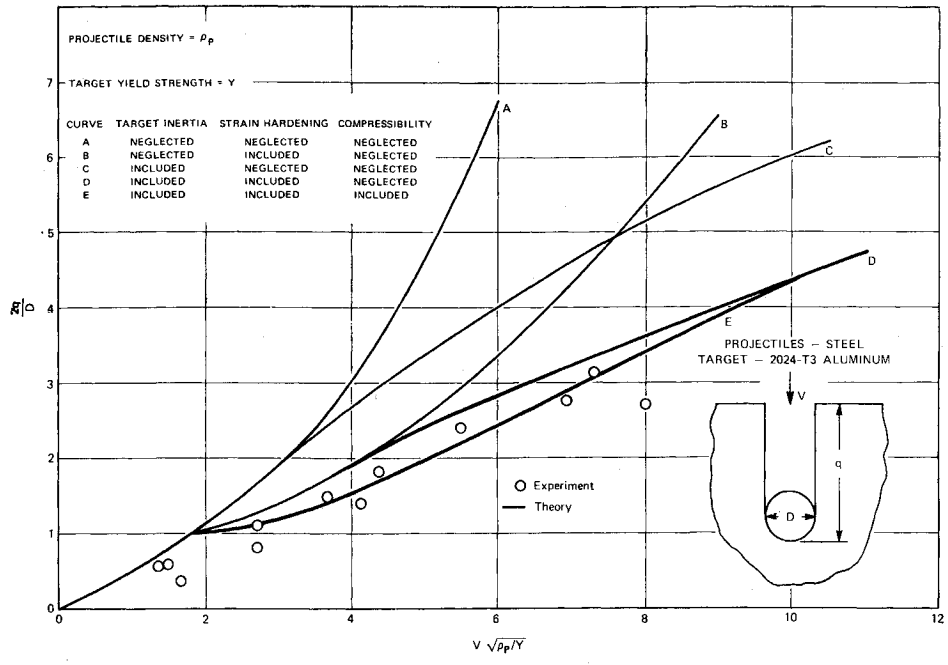

Fig. 3 Comparison between results of deep penetration theories and experimental data for hypervelocity impact of steel spherical projectiles in aluminum targets.

Eq. (65) results in

$$p(t) = \frac{2}{3}Y\left(1 + \ln\frac{2E}{3Y}\right) + \frac{2}{27}\pi^2 E_t - \frac{2}{3}Y\frac{E_t}{E} + \rho\left(a\ddot{a} + \frac{3}{2}\dot{a}^2\right) \quad (70)$$

It is noted that this expression for $p(t)$ corresponds identically to the similar relationship derived in Ref. 5 for an incompressible medium with the exception that Eq. (70) incorporates the extra term $-2YE_t/3E$. This term is obtained as a consequence of evaluating the present strain-hardening integral[6] over the truncated interval $1 > y \geq a^3/b^3$ in lieu of the limits $1 > y \geq 0$ assumed by Goodier. In this latter case, Goodier has postulated the same condition as Bishop, Hill, and Mott[2] for the upper limit of the strain-hardening integral; namely, that $b \to \infty$ and $a/b \to 0$. Although this assumption is rigorous for the incompressible, elastic-plastic medium, it does not follow when compactibility of the material is taken into account. Thus, if the ratio b/a is finite, Eq. (70) results and the dissonance with the Goodier solution is recognized.

Returning now to Eq. (65), which represents the more general case of a compactible medium that experiences ideal-locking behavior under hydrostatic stress, and elastic-plastic response in shear, and introducing the following notation:

$$p_s = \tfrac{4}{9}E(1 - e^{-3\beta}) - \tfrac{2}{3}Y\ln\delta + \tfrac{2}{2^7}\pi^2 E_t - \tfrac{4}{9}E_t\eta \quad (71a)$$

$$B_1 = 1 - \delta^{1/3} \quad (71b)$$

$$B_2 = \tfrac{3}{2} - (1 + \alpha_p)\delta^{1/3} + \tfrac{1}{2}\delta^{4/3} \quad (71c)$$

enables the complete expression for cavity pressure as a function of time to be written as

$$p(t) = p_s + \rho_{l_p}(B_1 a\ddot{a} + B_2\dot{a}^2) \quad (72)$$

As mentioned in Ref. 6 and explained by Goodier,[1,5] the symmetric spatial variation of dynamic pressure around the frontal surface of the penetrating sphere can be assumed to follow a cosine variation, so that stagnation pressure is obtained along the axis of penetration and zero normal pressure results at the horizontal diametral plane. Then, the effective dynamic force resisting penetration along the vertical axis is given by

$$\tfrac{2}{3}\rho_{l_p}[B_1 a\ddot{a} + B_2\dot{a}^2]\pi a^2 \quad (73)$$

Therefore, the equation of motion for a projectile of mass M and diameter D that is penetrating the target material in the vertical direction is

$$M\ddot{q} = -\left[p_s + \frac{2}{3}\rho_{l_p}\left(B_1\frac{D}{2}\ddot{q} + B_2\dot{q}^2\right)\right]\frac{\pi D^2}{4} \quad (74)$$

and after integration

$$\ln\left(p_s + \frac{2}{3}B_2\rho_{l_p}\dot{q}^2\right) = -\frac{4}{3}B_2\rho_{l_p} \times \frac{q}{\frac{M}{A} + B_1\frac{D}{3}\rho_{l_p}} + C_1 \quad (75)$$

Initial conditions can now be introduced to determine the constant of integration C_1. Specifically, the projectile penetration velocity can be taken as $v = v_0$ when $q = q_0$ where q_0 is the depth of penetration which defines the interface between shallow penetration theory and deep penetration theory phases.[1,5] Shallow penetration theory governs projectile motion in the target material through an indentation depth that corresponds to one-sphere radius (i.e., hemispherical submergence). The basic analysis is founded on dynamic hardness test concepts[7] and has been modified for penetration in compactible media by Ross and Hanagud.[6]

Substitution of these conditions in Eq. (75) and rearrangement yields

$$q_t = q_0 + \frac{3}{4}\frac{(M/A) + B_1(D/3)\rho_{l_p}}{B_2\rho_{l_p}}\ln\frac{p_s + \frac{2}{3}B_2\rho_{l_p}v_0^2}{p_s} \quad (76)$$

where terminal value of penetration depth $q = q_t$ has been obtained by setting the velocity $\dot{q}$ equal to zero.

Comparison of Theory and Experiment

Results of the present large deformation, deep penetration theory for a compactible medium have been used to provide a theoretical comparison with experimental data realized in hypervelocity impact tests. Findings of this effort are contained in Fig. 3, which concerns the hypervelocity impact of spherical steel projectiles in a target material of 2024-T3 Aluminum. In this case, the experimental data were obtained by Langley and Rheem at NASA Langley,[8] and the

theoretical curves denoted A through D were determined by Goodier[1,5] for the following projectile and target material properties: $E = 10.0 \times 10^6$ lb/in.^{2}, $Y = 56{,}000$ lb/in.^{2}, $E_t = 0.41 \times 10^6$ lb/in.^{2}, $\rho_p = 0.284$ lb/in.^{3}, $\rho_0 = 0.100$ lb/in.^{3} Under these conditions, the nondimensional quantity, $V[\rho_p/Y]^{1/2}$, which is used as an abscissa in the plot of Fig. 3, indicates a projectile impact velocity, $V = 7270$ fps, when $V[\rho_0/Y]^{1/2} = 10$.

It is noted that Curve D, which was obtained from the Goodier deep penetration theory for an incompressible medium, includes the significant effects of target inertia and strain hardening. Here, Goodier states that "the agreement with experimental points is fair, suggesting that the theory has taken account of the most important governing properties and merits further examination." Apropos these comments, Curve E, which was obtained from the present deep penetration theory and includes the effects of target material compressibility, is observed to provide a better fit with experimental data than heretofore available.

Specifically, the Goodier theory predicts penetration depths that are somewhat higher than those provided by both the present theory and experiment. This discrepancy is more pronounced in earlier stages of the deep penetration phase; that is, just following completion of the shallow penetration phase over a velocity range, $2.50 < V[\rho_p/Y]^{1/2} < 5.50$. It is interesting to note that predictions of the Goodier theory are also higher than experimental values by the same order-of-magnitude in cases where test data were realized for copper and lead projectiles.[1]

In determining Curve E from the present theory it was necessary to employ data characterizing the compressibility behavior of the aluminum target material at high rates of loading. For this purpose, use was made of the Hugoniot data published by Fowles[9] for the shock wave compression of hardened and annealed aluminum.

Calculations were carried out within the range of interest by first choosing discrete values of projectile striking velocity. This quantity, which after impact with the target material corresponds to particle velocity behind the outward propagating shock front, was then referred to the appropriate stress-particle velocity curve to obtain compressive stress under shock loading. Use of this quantity in conjunction with the corresponding stress-specific volume curve provided, by inversion, an associated value of density for the compressed material at the cavity surface which was then averaged with the initial density value characterizing material at the shock front to define the locking density ρ_{l_p} of material surrounding the penetrating projectile. In this manner, individual values of locking density were obtained as a function of projectile impact velocity and employed subsequently in calculations to obtain the terminal penetration depth relationship portrayed in Fig. 3.

Penetration depths predicted by the present theory for $2 \leq V[\rho_p/Y]^{1/2} < 7$ are less than those obtained by the incompressible theory. This is expected because resistance to penetration at lower impact velocities is contributed mainly by the shock wave effect, wherein material behind the advancing front is compressed over its initial, stress-free value. For example, when $V[\rho_p/Y]^{1/2} = 4$, a compaction of 12% is obtained. At higher impact velocities, the compactibility effect increases (in fact when $V[\rho_p/Y]^{1/2} = 10$, 23% compactibility obtains); however, due to coupled high-pressure effects, the target material also behaves more like a fluid and tends to lose its shear resistance to penetration. Since the incompressible material also exhibits this type of fluid behavior at high impact velocities, the disparity between theories dissolves. Moreover, the simple averaging technique used to calculate locking density is no longer accurate at these higher impact velocities and associated large compressibility factors. In this connection, it is pointed out that Curve E is not asymptotic to Curve D but actually crosses over to predict higher penetration depth for the compressible case. For this region, the present theory is probably inadequate; however, comparison with experiment is not attempted at these velocities.

Lastly, results obtained from the present theory have been employed also to effect comparisons with experimental data realized in projectile and bomb penetration tests over a range of velocities characterizing free-fall impact (0–1000 fps). This work is presented in Ref. 6 where it is noted that agreement between theory and experiment was very good in all cases.

References

[1] Goodier, J. N., "On the Mechanics of Indentation and Cratering in Solid Targets of Strain-Hardening Metal by Impact of Hard and Soft Spheres," TR 002-64, July 1964, Poulter Laboratories, Stanford Research Institute, Menlo Park, Calif.

[2] Bishop, R. F., Hill, R., and Mott, N. F., "The Theory of Indentation and Hardness Tests," *Proceedings, Physical Society of London*, Vol. 57, 1945, pp. 147–159.

[3] Hopkins, H. G., "Dynamic Expansion of Spherical Cavities in Metals," *Progress in Solid Mechanics*, Vol. 1, edited by R. Hill and I. N. Sneddon, Pergamon Press, Oxford, England, 1960, pp. 84–164.

[4] Hanagud, S., "Finite Amplitude Spherical Waves in a Locking-Relaxing Solid," Invited Research Lecture, *Proceedings, 5th U.S. National Congress of Applied Mechanics*, American Society of Mechanical Engineers, 1966, pp. 63–77.

[5] Goodier, J. N., "On the Mechanics of Indentation and Cratering in Solid Targets of Strain-Hardening Metal by Impact of Hard and Soft Spheres," *Proceedings, 7th Symposium on Hypervelocity Impact*, Vol. III, AIAA, New York, 1965, pp. 215–259.

[6] Ross, B. and Hanagud, S., "Penetration Studies of Ice with Application to Arctic and Subarctic Warfare," Final Rept. NWRC 7000-452-4, Contract N00014-68-A-0243, Sept. 1969, Stanford Research Institute, Menlo Park, Calif.

[7] Tabor, D., *The Hardness of Metals*, Oxford Press, Oxford, England, 1951.

[8] Herrman, W. and Jones, A. H., "Survey of Hypervelocity Impact Information," Rept. 99-1, Sept. 1961, M.I.T. Aeroelastic and Structures Research Laboratory, Cambridge, Mass.

[9] Fowles, G. R., "Shock Wave Compression of Hardened and Annealed 2024 Aluminum," TR 011-60, Oct. 1960, Poulter Laboratories, Stanford Research Institute, Menlo Park, Calif.